Assessment of cameras for continuous wave sub-terahertz imaging

Andrei Gorodetsky[1,2], Suzanna Freer[1], and Miguel Navarro-Cía[1]

[1]School of Physics and Astronomy, University of Birmingham, Birmingham B15 2TT, UK
[2]ITMO University, St. Petersburg 197101, Russia

ABSTRACT

In this contribution, we present the direct comparison between Ophir Pyrocam IV and Terasense Tera-1024 cameras used for imaging of terahertz (THz) and sub-THz signals. We compare general properties, such as frequency dependent and polarisation dependent sensitivity, angle dependent sensitivity essential for holographic and noncollinear interferometric measurements, and draw a conclusion about the most suitable camera for the discussed imaging approaches. Both cameras show acceptable performance and sensitivity at imaging both 0.14 THz and 0.3 THz signals. The Terasense camera, expectedly, shows stronger polarisation dependent properties, however, is significantly more angle independent, showing an acceptable performance at all tested incident angles up to 50 degrees. At the same time, although the angle dependence is stronger for the Ophir camera, it has smaller pixel pitch and more extended post-processing features, thus making it somewhat better suited for noncollinear interferometric and holographic sub THz imaging.

Keywords: THz imaging, THz cameras

1. INTRODUCTION

THz frequency range used to be and sometimes still is called 'a gap',[1] because of the absence of controlled transcievers in the range, as the frequencies are too high for typical electronics (electron motion based sources), and photon energies are too low for typical quantum systems (electron transition based sources). This turns the THz science into a catch-up research field, where all the technologies and methods developed for neighbouring microwave and optical spectral ranges can potentially be, with varying degrees of success, transferred into the THz methods, and imaging will not be an exclusion.

The growing need for fast yet precise terahertz (THz) imaging setups has become an actual task in the recent years. The appearance of rather compact yet efficient THz and sub-THz sources[2] has paved the way for realtime THz and sub-THz imaging. Favourable properties of THz radiation, such as its abilily to petentrate optically opaque substances, low photon energy and extreme sensitivity to water content[3] as well as the ability for remote measurement of ultrafast conductivity[4] are the key features for numerous applications in nondestrutive testing, intravision and biomedical imaging.[5]

Sub-THz imaging systems based on impact ionization transit time (IMPATT) diodes and plasmonic array detectors[6] offered by Terasense arguably are the best tool for realtime imaging applications in the sub-THz spectral range between 50 and 300 GHz available on the market.[7,8] They offer reasonable sensitivity, resolution, and speed of operation, yet are rather compact, energy efficient and easy in installation. However, they require precise alignment of the numerous quasi optical elements and can not provide both high resolution and stand-off operation simultaneously. Moreover, these systems still suffer from diffraction effects and low resolution imposed by the wavelength of the radiation used. In numerous biomedical applications,[9] higher spatial resolution is strongly desired.

On the one hand, raising the imaging resolution can be achieved by migrating the technology to the smaller wavelength range in the electromagnetic spectrum. On the other hand, such a shift might be technically complex if not impossible - THz technology is already working beyond the typical technological limits. Multiplication of

Further author information: (Send correspondence to M.N.-C.)
M.N.-C.: E-mail: M.Navarro-Cia@bham.ac.uk

the electronically generated frequency results in drastic drop of its power. Moreover, atmospheric absorption of the radiation at frequencies above 0.7 THz becomes prominent.[10] Hence, there is a request for other approaches to spatial resolution enhancement in THz imaging.

Most well-known imaging techniques, providing either outstanding resolution, or high speed operation, or full wavefront resonstruction, such as near field imaging,[11] compressed sensing[12] or holographic phase retrieval[13] have been already demonstrated. For many of these techniques, requiring non-collinear beam alignment, a knowledge of the detector properties, especially, its angular, spectral and polarization sensitivity are essential for efficient imaging system design and implementation.

Here, we present the characterisation of the two most widely used uncooled matrix detectors of THz radiation: Ophir Pyrocam IV and Terasense cameras. We compare their general properties, such as spectral sensitivity, response to polarization and angular susceptibility, essential for holographic and noncollinear interferometric measurements.

2. EXPERIMENTAL SETUP

The experimental setup used in this study consisted of four basic components: a sub-THz source, a focusing lens in a 2-f layout to allow direct imaging of the source onto the camera, camera under characterisation, and the rotation stage that camera is mounted onto.

The layout of the setup is presented in Fig. 1.

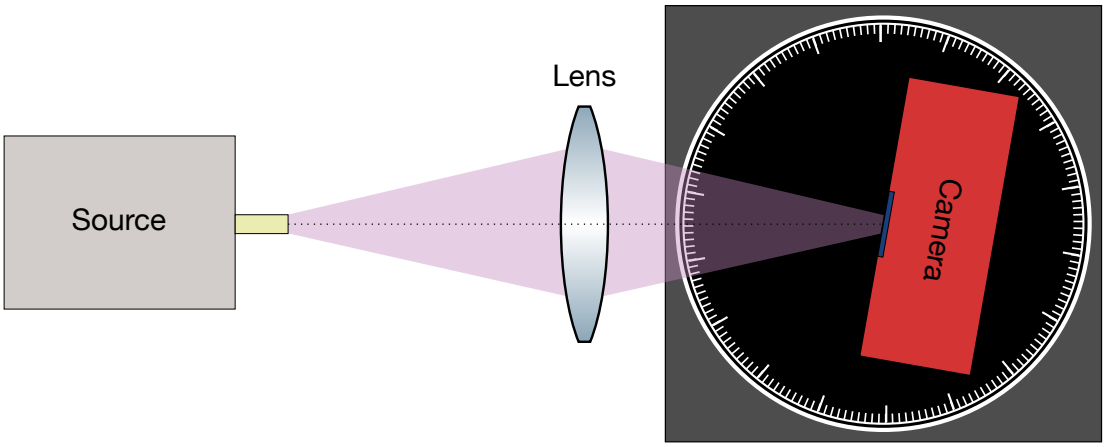

Figure 1. General layout of the assessment setup.

To study the THz cameras operational characteristics, two different sources of sub THz radiation made by Terasense were used, namely, 140 GHz and $\sim$ 300 GHz (actual frequency is 292 GHz) sources. The 140 GHz source has a detachable conical horn antenna output and the $\sim$ 300 GHz source has a detachable diagonal horn antenna.

The cameras under study are Tera-1024 plasmonic camera from Terasense and Pyrocam IV pyroelectric camera from Ophir. The camera datasheet characteristics are given in Table 1.

Table 1: Cameras under study detailed characterstics.

Parameter	**Tera-1024**	**Pyrocam IV**
Operational wavelengths	430 μm – 6000 μm	1.06 μm – 3000 μm
Operational frequencies	0.05 – 0.7 THz	0.1 – 283 THz
Sensor size	48×48 mm	25.6×25.6 mm
Resolution	32×32 pixels	320×320 pixels
Pixel pitch	1.5 mm	80 μm
NEP	$\frac{1\ \text{nW}}{\sqrt{\text{Hz}}}$	$\frac{13\ \text{nW}}{\sqrt{\text{Hz}} \cdot \text{pixel}}$
Responsivity	$50\frac{\text{kV}}{\text{W}}$	N/A
Sensitivity	N/A	$\frac{64\ \text{nW}}{\text{pixel}}$
Physical size	$11.5 \times 11.5 \times 4.2$ cm	$14.7 \times 14.7 \times 5.5$ cm
PC interface	USB	Gigabit Ethernet

From the characteristics, it can be seen that both cameras successfully work with the sources involved. Pyrocam offers a much smaller detection area, but significantly finer pixel pitch that comes at the price of lower single pixel sensitivity. We would like to note that although Tera-1024 camera is sensitive across the full spectral range in the Table 1, its sensitivity is not even, but has maxima around 140 GHz multiples, i.e. 70 GHz, 140 GHz, 280 GHz, etc, while response of the Pyrocam in that range is relatively flat. On the other hand, Pyrocam is sensitive to visible light (this is not stated in our Table 1 to avoid addlement), which means one should work with this camera in completely dark environment.

To study angular and polarization camera sensitivity, the cameras were mounted on a rotational stage (see Fig. 1), with the centre of the sensor aligned with the stage axis. It is worth noting that both cameras do not give the user direct opportunity to do this, as mounting threads are not aligned to the sensor plane, or its centre.

Both cameras were tested with both 140 GHz and ~ 300 GHz sources at 4 different oprientational combinations - i) Source vertical, camera vertical, ii) Source vertical, camera horizontal, iii) Source horizontal, camera vertical, and iv) Source horizontal, camera horizontal, while camera rotation was done in the same plane to assure probing angular sensitivity in both directions and polarization states.

The BeamGage software that comes with the Pyrocam offers far more options and analysis tools than the software for Terasense. It allows the user to set exposure time and sensitivity separately. Also, it allows for averaging the data and analysis (e.g. Gaussian and other beamwaist and amplitude estimation necessary for this characterisation and much more), while Terasense software gives only one sensitivity setting to the user, and the ratio between neigbouring settings of this parameter is unexplained, which makes it difficult to use for quantitative measurements. For the characterisation, the Pyrocam was used in the CW regime, with built-in chopper operating at 25 Hz. Sensitivity and exposure settings were adjusted for the set of measurements to avoid overshoot at normal incidence and were kept unchanged afterwards. Similar setting was applied to the Terasense's sensitivity setting. The output data of the cameras also vary: Terasense operates at 8-bit, while Pyrocam offers 15-bit data and 1000:1 dynamic range measurement. For high signals, this can be a tremendous advantage, especially for interferometric and holographic imaging applications.

For both cameras, two beam parameters were retrieved: the maximum value at the sensor, and the amplitude of the Gaussian fitting to the detected beam. Due to strong interference in the setup, it was not always possible to fit the beam with a Gaussian beam distribution.

3. EXPERIMENTAL RESULTS

3.1 140 GHz source

The beam profiles recorded by the two cameras under study at normal operational orientation for the radiation of the 140 GHz source are shown in Figure 2.

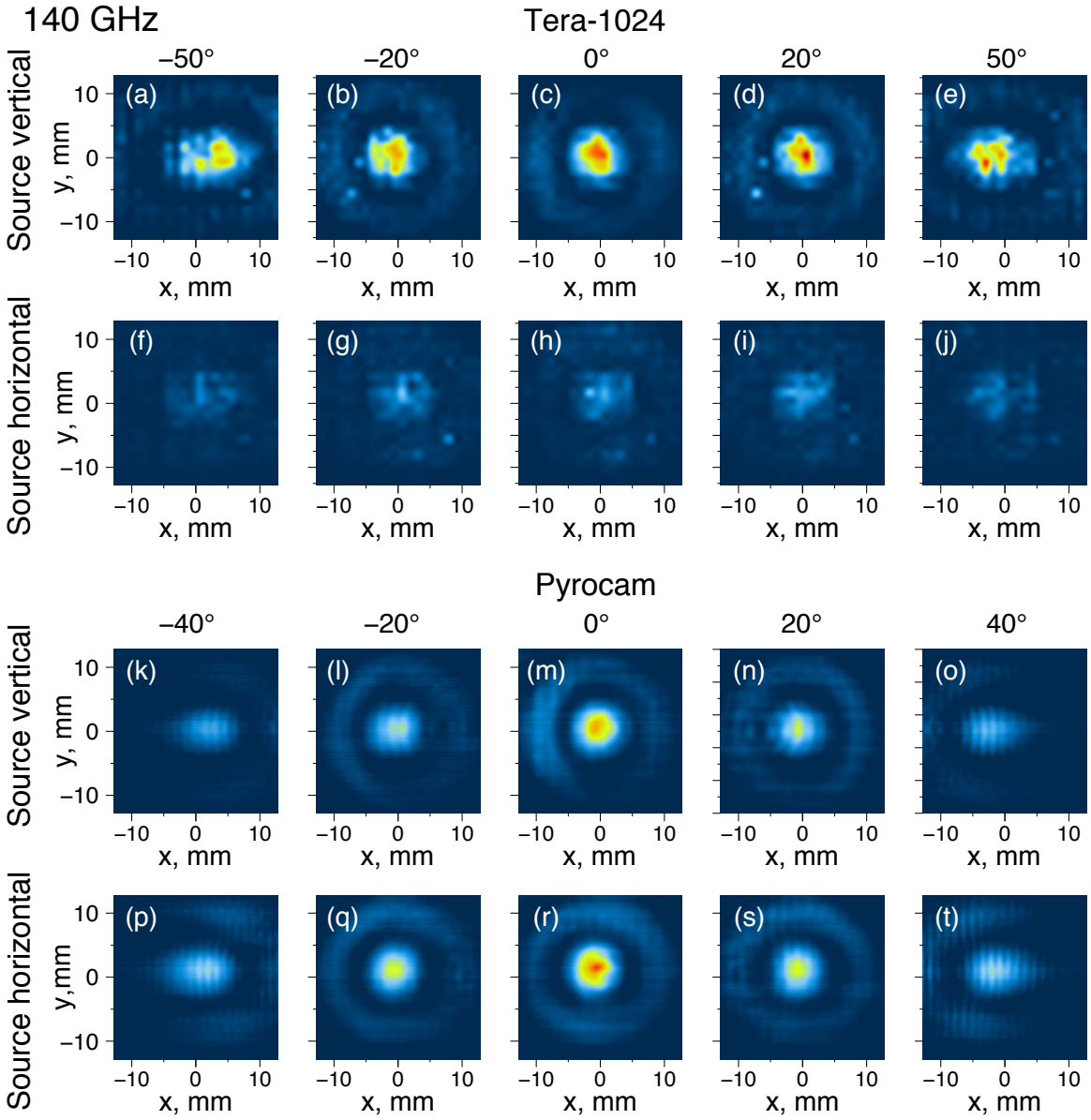

Figure 2. Angle dependent sensitivity of cameras detecting radiation from 140 GHz IMPATT diode. (a) – (e) – Tera-1024 oriented parallel to the source, (f) – (j) – Tera-1024 oriented perpendicularly to the source, (k) – (o) – Pyrocam oriented parallel to the source, (p) – (t) – Pyrocam oriented perpendicularly to the source, for angles from –50 (–40 for Pyrocam) to 50 (40 for Pyrocam), correspondingly.

Figure 2 (a)–(e) presents the beam profiles recorded by the Tera-1024 camera, with the 140 GHz source emitting vertical (normal operational) polarization upon camera rotation from −50° to 50°, Figure 2 (f)–(j) presents the beam profiles recorded by the Tera-1024 camera, with the 140 GHz source emitting horizontal (orthogonal) polarization upon camera rotation from −50° to 50°, Figure 2 (k)–(o) presents the beam profiles

recorded by the Pyrocam camera, with the 140 GHz source emitting vertical (normal operational) polarization upon camera rotation from −40° to 40°, and Figure 2 (p)–(t) presents the beam profiles recorded by the Pyrocam camera, with the 140 GHz source emitting horizontal (orthogonal to typical operational) polarization upon camera rotation from −40° to 40°.

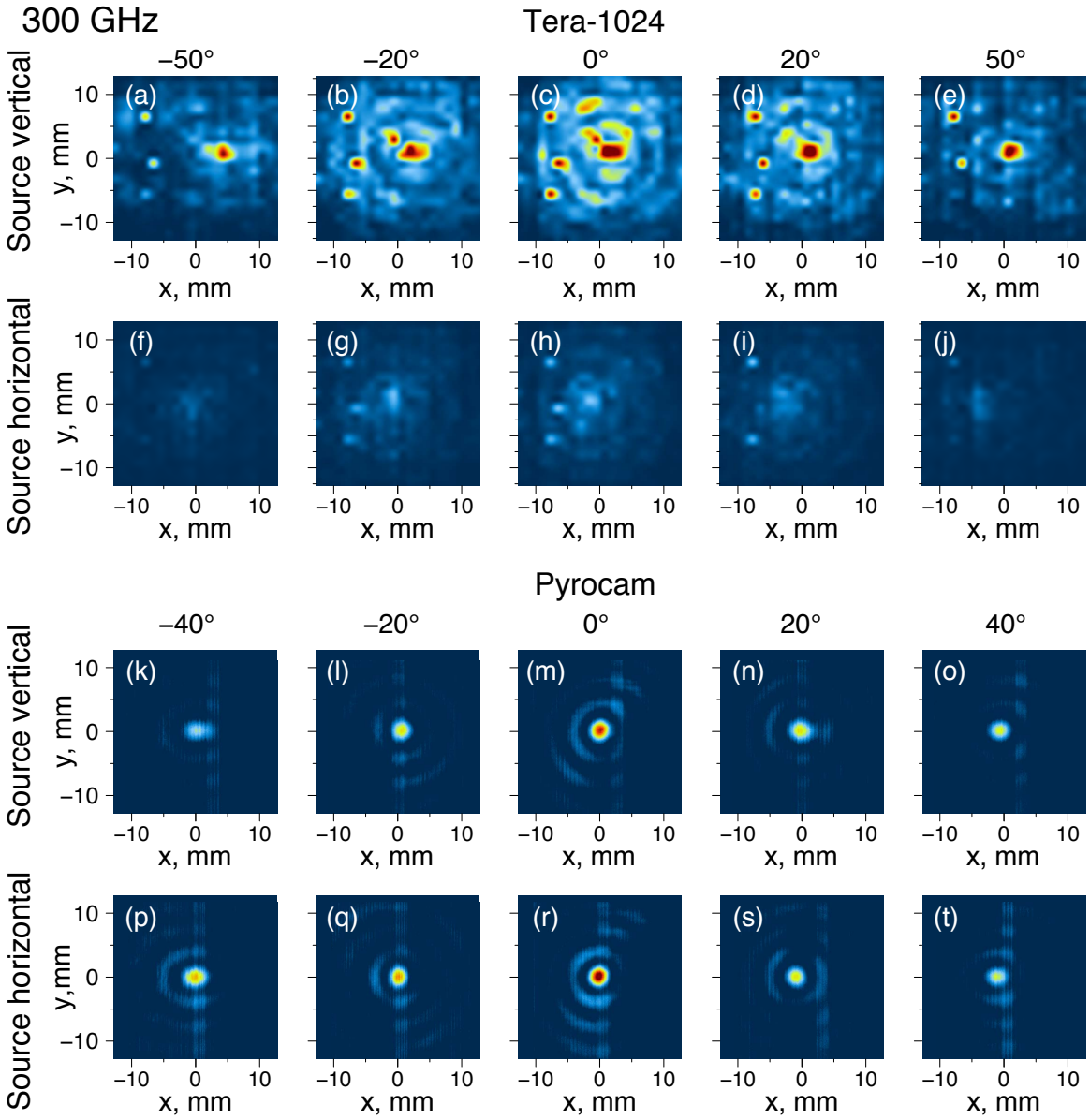

Figure 3. Angle dependent sensitivity of cameras detecting radiation from ∼ 300 GHz IMPATT diode. (a) – (e) – Tera-1024 oriented parallel to the source, (f) – (j) – Tera-1024 oriented perpendicularly to the source, (k) – (o) – Pyrocam oriented parallel to the source, (p) – (t) – Pyrocam oriented perpendicularly to the source, for angles from –50 (–40 for Pyrocam) to 50 (40 for Pyrocam), correspondingly.

From the figure, it can be seen that both cameras provide quite similar beam profiles at all angles. Secondly, Tera-1024 possesses severe polarisation sensitivity, which is not present in the Pyrocam images. Interference rings coming from the finite size source Fourier imaged onto the camera are present in all the pictures. Vertical interference fringes noticeable in the Pyrocam pictures of the beam (Figure 2 (k,o,p,t)) are, most likely, coming

from the scattering off the edge of the camera. The Pyrocam sensing matrix is situated deeper inside the camera body, while in the case of Tera-1024 it is placed immediately at its front face. For the same reason, we could not characterise Pyrocam at angles beyond −40° to 40°, because edge diffraction effects took over the intensity distribution pattern.

3.2 ∼ 300 GHz source

Similarly, beam profiles recorded by the two cameras under study at normal operational orientation of both cameras for the radiation of the ∼ 300 GHz source are shown in Figure 3.

Figure 3 (a)–(e) presents the beam profiles recorded by the Tera-1024 camera, with the ∼ 300 GHz source emitting vertical (normal operational) polarization upon camera rotation from −50° to 50°, Figure 3 (f)–(j) presents the beam profiles recorded by the Tera-1024 camera, with the ∼ 300 GHz source emitting horizontal (orthogonal) polarization upon camera rotation from −50° to 50°, Figure 3 (k)–(o) presents the beam profiles recorded by the Pyrocam camera, with the ∼ 300 GHz source emitting vertical (normal operational) polarization upon camera rotation from −40° to 40°, and Figure 3 (p)–(t) presents the beam profiles recorded by the Pyrocam camera, with the ∼ 300 GHz source emitting horizontal (orthogonal to typical operational) polarization upon camera rotation from −40° to 40°.

From the figure, it can be seen that both cameras provide rather comparable beam profiles at all angles. The power of ∼ 300 GHz source is almost 10 times lower, resulting in reduced signal/noise values, especially visible in the Tera-1024 device (sensitivity was adjusted for both cameras). Similarly to the results for 140 GHz, Tera-1024 possesses severe polarisation sensitivity, absent in the Pyrocam. Interference rings are much more narrow and frequent, due to a smaller wavelength, and are not fully resolved by the Tera-1024, becasue of its larger pixel pitch. Similarly, an achievable beamwaist is much smaller, as well as vertical interference fringes noticeable in Pyrocam pictures of the beam (Figure 3 (k,o,p,t)).

3.3 Comparison of the beam profiles

To demonstrate contrast and outline the sensing performance of the cameras, we show the beam cross-sections at 0° for both the 140 GHz and ∼ 300 GHz sources. These cross-sections are shown in Figure 4.

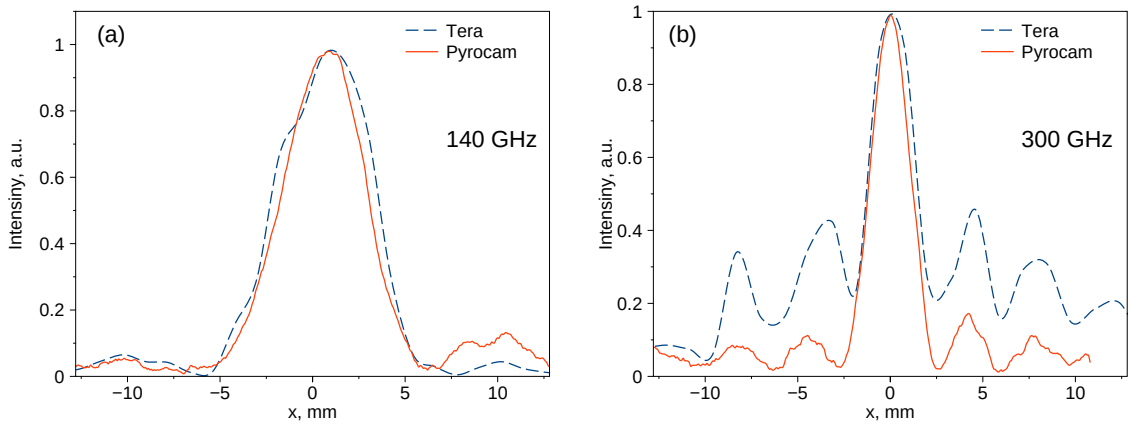

Figure 4. Cross sections of the captured beam profiles at (a) 140 GHz and (b) ∼ 300 GHz.

Figure 4 shows a very decent correspondence of the profiles obtained with both cameras at both frequncies. Pixel pitch of Tera-1024 seems to be too large (1.5 mm) to fully resolve interference fringes of the ∼ 300 GHz source (∼ 1 mm wavelength). Thus, for holographic and interferometric imaging with the ∼ 300 GHz source, only the Pyrocam can be recommended, as the Tera-1024 does not provide interference fringe resolution with full contrast. For imaging with the 140 GHz source and lower frequency sources, the Tera-1024 can be recommended, as it has a larger area, essential for finer resolution. Moreover, Terasense offers an even larger Tera-4096 camera and linear detector, covering even larger numerical apertures.

3.4 Comparison of the angular sensitivity.

Finally, we quantitatively compare camera operation under non-normal angles of incidence, as such layouts are rather typical in holographic and interferometric imaging setups.[13,14] As outlined in Figure 1, the cameras were rotated about the axis going through the centre of the sensor, to avoid shifting of the beam across the sensor area. Rotation was performed with 2° steps, for angles ranging from −50° to 50° for the Tera-1024 camera and from −40° to 40° for the Pyrocam, as larger angles were not allowed by the diffraction on the entrance aperture. Rotation was performed at both normal operational and orthogonal camera positions. The results are shown in Figure 5, where the maximum value of the registered beam profile (marked as Center and plotted with the dashed line) and the amplitude of the Gaussian fit to the central lobe (marked as Gaussian and plotted with the solid line) are shown. Note that sensitivity curves are plotted in linear scale.

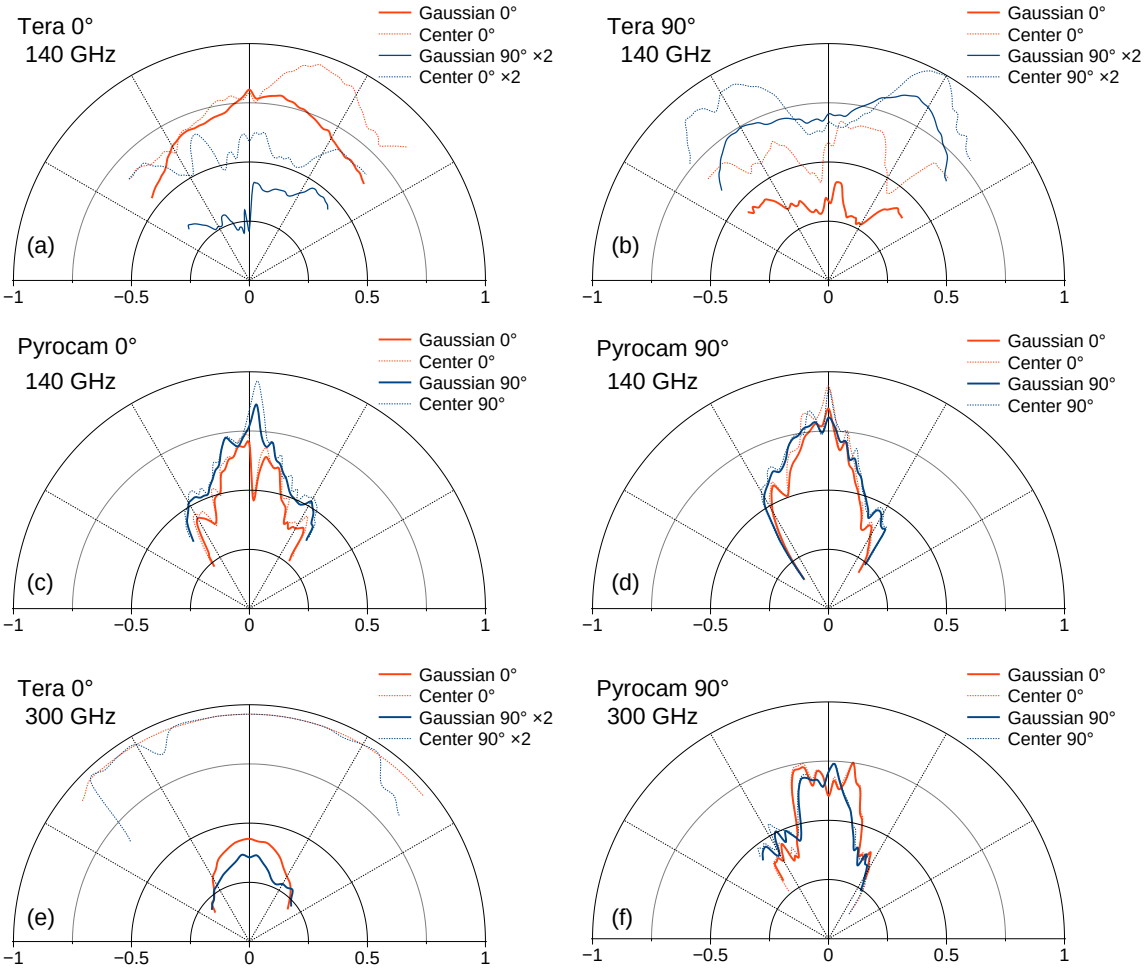

Figure 5. Angle dependent sensitivity of cameras detecting radiation from 140 GHz and ∼ 300 GHz IMPATT diodes. (a) – Tera-1024 in normal operational orientation imaging 140 GHz source, (b) – Tera-1024 in orthogonal orientation imaging 140 GHz source, (c) – Pyrocam in normal operational orientation imaging 140 GHz source, (d) – Pyrocam in orthogonal orientation imaging 140 GHz source, (e) – Tera-1024 in normal operaional orientation imaging ∼ 300 GHz source, (f) – Pyrocam in orthogonal orientation imaging ∼ 300 GHz source. Data for source's normal operational orientation are plotted in red, orthogonal source's orientation in blue. Dashed lines show the maximum of the intensity pattern, while solid lines show the amplitude of the Gaussian fitting to the central lobe.

The plots in Figure 5 reveal several trends in angle dependences. First, Tera-1024 is almost insensitive to the incident angle, as the signal falls only by 20% upon rotation from 0° to ±50°. Moreover, orthogonal position characterisation reveals the sidelobes of camera sensitivity at about ±30°. The Pyrocam signal, in contrast,

shows significant angle dependence, as the sensitivity falls aproximately 4 times upon rotation from 0° ±40°, and shows no significant difference due to the polarisation.

4. CONCLUSION

In this work, we considered the two commercially available cameras for sub-THz imaging. We studied their applicability for noncollinear holographic and interferometric THz imaging. While giving more freedom in settings and finer pixel pitch, Pyrocam IV has a smaller sensor and suffers from strong angular sensitivity dependence. Tera-1024, in contrary, does not allow full interferometric registration of $\sim$ 300 GHz radiation and has lower contrast, but is quite robust to the angle of incidence and has larger area and higher sensitivity, especially to sources with lower frequrency. We conclude that Tera-1024 (and its modifications, especially ones having a larger area) are better suited for holographic and interferometric imaging with lower frequency (140 GHz and below) sources, while Pyrocam IV, currently, is the only performer for imaging with radiation at frequencies of $\sim$ 300 GHz and above.

ACKNOWLEDGMENTS

This work was supported in part by the EPSRC [Grant No. EP/S018395/1] and the Royal Society [Grant No. IES/R3/183131 and IEC/NSFC/191104]. AG thanks Magicplot LLC for providing a copy of MagicPlot Pro plotting and fitting software.

REFERENCES

[1] Williams, G. P., "Filling the THz gap—high power sources and applications," *Reports Prog. Phys.* **69**(2), 301–326 (2006).

[2] Dhillon et al., S. S., "The 2017 terahertz science and technology roadmap," *J. Phys. D. Appl. Phys.* **50**(4), 043001 (2017).

[3] Taylor, Z. D., Garritano, J., Sung, S., Bajwa, N., Bennett, D. B., Nowroozi, B., Tewari, P., Sayre, J. W., Hubschman, J.-P., Deng, S. X., Brown, E. R., and Grundfest, W. S., "THz and mm-Wave Sensing of Corneal Tissue Water Content: In Vivo Sensing and Imaging Results," *IEEE Trans. Terahertz Sci. Technol.* **5**(2), 184–196 (2015).

[4] Beard, M. C., Turner, G. M., and Schmuttenmaer, C. A., "Transient photoconductivity in GaAs as measured by time-resolved terahertz spectroscopy," *Phys. Rev. B* **62**(23), 15764–15777 (2000).

[5] Smolyanskaya, O., Chernomyrdin, N., Konovko, A., Zaytsev, K., Ozheredov, I., Cherkasova, O., Nazarov, M., Guillet, J.-P., Kozlov, S., Kistenev, Y. V., Coutaz, J.-L., Mounaix, P., Vaks, V., Son, J.-H., Cheon, H., Wallace, V., Feldman, Y., Popov, I., Yaroslavsky, A., Shkurinov, A., and Tuchin, V., "Terahertz biophotonics as a tool for studies of dielectric and spectral properties of biological tissues and liquids," *Prog. Quantum Electron.* **62**, 1–77 (2018).

[6] Muravev, V. M. and Kukushkin, I. V., "Plasmonic detector/spectrometer of subterahertz radiation based on two-dimensional electron system with embedded defect," *Appl. Phys. Lett.* **100**(8), 082102 (2012).

[7] Tzydynzhapov, G., Gusikhin, P., Muravev, V., Dremin, A., Nefyodov, Y., and Kukushkin, I., "New Real-Time Sub-Terahertz Security Body Scanner," *J. Infrared, Millimeter, Terahertz Waves* (2020).

[8] Shchepetilnikov, A. V., Gusikhin, P. A., Muravev, V. M., Tsydynzhapov, G. E., Nefyodov, Y. A., Dremin, A. A., and Kukushkin, I. V., "New Ultra-Fast Sub-Terahertz Linear Scanner for Postal Security Screening," *J. Infrared, Millimeter, Terahertz Waves* (2020).

[9] Smirnov, S. V., Grachev, Y. V., Tsypkin, A. N., and Bespalov, V. G., "Experimental studies of the possibilities of diagnosing caries in the solid tissues of a tooth by means of terahertz radiation," *J. Opt. Technol.* **81**(8), 464 (2014).

[10] Yang, Y., Shutler, A., and Grischkowsky, D., "Measurement of the transmission of the atmosphere from 0.2 to 2 THz," *Opt. Express* **19**(9), 8830 (2011).

[11] Cocker, T. L., Jelic, V., Gupta, M., Molesky, S. J., Burgess, J. A. J., Reyes, G. D. L., Titova, L. V., Tsui, Y. Y., Freeman, M. R., and Hegmann, F. A., "An ultrafast terahertz scanning tunnelling microscope," *Nat. Photonics* **7**(8), 620–625 (2013).

[12] Chan, W. L., Charan, K., Takhar, D., Kelly, K. F., Baraniuk, R. G., and Mittleman, D. M., "A single-pixel terahertz imaging system based on compressed sensing," *Appl. Phys. Lett.* **93**(12), 121105 (2008).

[13] Valzania, L., Zhao, Y., Rong, L., Wang, D., Georges, M., Hack, E., and Zolliker, P., "THz coherent lensless imaging," *Appl. Opt.* **58**(34), G256 (2019).

[14] Neumann, A., Kuznetsova, Y., and Brueck, S. R. J., "Optical resolution below $\lambda/4$ using synthetic aperture microscopy and evanescent-wave illumination.," *Opt. Express* **16**(25), 20477–20483 (2008).